WATER RESOURCES RESEARCH, VOL. 37, NO. 8, PAGES 2103–2111, AUGUST 2001

Approximate boundaries between different flow regimes in fractured rocks

Tetsu K. Tokunaga and Jiamin Wan

Earth Sciences Division, Lawrence Berkeley National Laboratory, Berkeley, California

Abstract. Recent studies have shown how water films at near-zero matric potentials on fracture surfaces could permit fast flow in unsaturated fractures. The present work is aimed at delineating the ranges of conditions necessary to permit film flow. The approximate matric potential needed to permit thickening of water films on fracture surfaces was estimated through correlating air-entry matric potentials and permeabilities for a wide range of porous media. An upper matric potential limit, associated with saturating the fracture, was related to the fracture aperture. These two limits, one dependent on matrix permeability and the other on fracture aperture, delineate the matric potential range within which thick water films develop on fracture surfaces. Rocks with matrix permeabilities less than $\sim 10^{-14}$ m^2, and fractures with apertures greater than ~ 30 μm permit some matric potential range over which thick water films can form. Highly transmissive films can develop on fracture surfaces only under near-zero matric and pressure potentials.

1. Introduction

Water moves through unsaturated, fractured rock by a complex combination of processes including slow flow within rock matrix blocks and potentially fast flow within fractures. The capacity of fractures for supporting fast flow and transport through the vadose zone has generated considerable research activity, much of which is being motivated by practical concerns over contaminant transport and groundwater contamination. Yet the spatial and temporal complexity of infiltration and seepage in fracture rocks continue to challenge our ability to develop a comprehensive understanding of these systems. A number of processes and models have been proposed to account for various facets of unsaturated zone flow in fractures, including flow through saturated aperture pathways [*Wang and Narasimhan*, 1985], episodic saturated flow [*Nitao and Buscheck*, 1991; *Wang et al.*, 1993], gravity-driven instabilities and flow fingering [*Nicholl et al.*, 1994], free surface film flow [*Kapoor*, 1994], matric film flow [*Tokunaga and Wan*, 1997; *Or and Tuller*, 2000], modified invasion percolation [*Glass et al.*, 1998], and intermittent flow [*Su et al.*, 1999]. Of the aforementioned phenomena, only film flows are explicitly restricted to truly unsaturated pathways within fractures. We use the term "film" in a macroscopic sense, to include both true water films on topographic maxima of fracture surfaces, and pendular, capillary water occupying topographic minima. We will refer to such water films on rough surfaces as "thick films" because they are substantially thicker than water films adsorbed onto flat, hydrophilic mineral surfaces. These latter films range in thickness from tens of nanometers to ~ 1 μm [*Pashley*, 1980; *Muller*, 1998] over a range of chemical potentials equivalent to the matric potentials we investigated in our previous and present work.

In view of the finding that film flow can occur, it is important to delineate necessary conditions associated with this process. It is desirable to identify a minimum number of factors necessary to predict the occurrence of film flow. On the basis of our previous work [*Tokunaga and Wan*, 1997], it is evident that the matric potential at the fracture surface must be high enough (close enough to zero) to bring the rock surface matrix (but not necessarily the bulk rock matrix) to its satiated water content. At the satiated water content, further increases in the matric potential (toward zero) result in insignificant increases in matrix saturation. Incomplete saturation is commonly observed under satiated conditions because of entrapped gas [*Klute*, 1986]. The bulk rock matrix is not necessarily satiated since it may have different hydraulic characteristics than those of rock surface regions. More generally, when true steady state conditions are not established, the rock matrix along fracture flow pathways may exist under satiated conditions while satiation of the interior matrix lags behind because of transport limitations. Nevertheless, when focusing on local fracture conditions, the satiation matric potential of the rock matrix remains a useful indicator of a lower energy limit above which film flow can occur. However, the satiation matric potential is neither a unique energy (because of hysteresis and nonspecific experimental equilibration time) nor a routinely measured parameter. Therefore it will be desirable to identify a more commonly measured rock property to correlate with matrix satiation. The matrix permeability can serve this purpose, as discussed below.

As the matric potential is increased above the matrix-satiation value, closer toward zero, water films become progressively thicker. An upper limit of film thickening is reached whereupon the fracture aperture becomes locally saturated. Given specific values of local hydraulic properties (matrix permeability and fracture aperture), there will generally be a lower limit in matric potential (Ψ_L) below which thick films are absent and an upper matric potential limit above which the local fracture aperture becomes fully water saturated (Ψ_U). Film flow is possible between these two energy limits (Figure 1). In this study, we seek to estimate the matric potential limits on film flow imposed by the combination of rock matrix permeability and fracture aperture size.

Paper number 2001WR000245.
0043-1397/01/2001WR000245$09.00

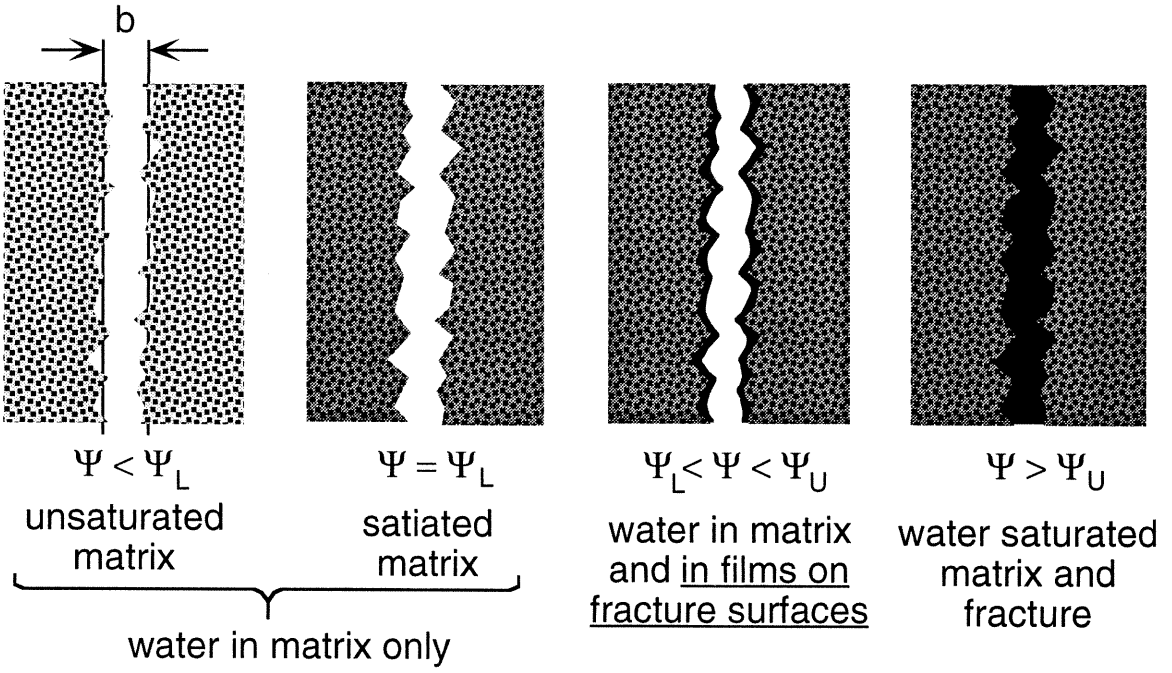

Figure 1. Conceptualization of the possible, matric potential-dependent distribution of water in fractured porous media. At matric potentials lower than ψ_L, water is retained in the unsaturated porous rock matrix. At ψ_L the matrix rock is effectively saturated. Between ψ_L and ψ_U, thick water films can develop along fracture surfaces, coexisting with the gas phase. Above ψ_U, the fracture aperture is fully (locally) saturated.

In this analysis, film flow in very large aperture fractures (greater than a few millimeters) is only considered in a limited manner. Although very thick water films can occur in very large aperture fractures, we restrict our discussions to films that are still thin enough to exist at finite (negative, but inclusive of near-zero) matric potentials, rather than under slightly positive pressure potentials. The upper limit in thickness of films at near-zero matric potentials is strongly dependent on local fracture surface topography. In our previous studies [*Tokunaga and Wan*, 1997; *Tokunaga et al.*, 2000], approximate upper limits in average film thickness ranged from 10 to 70 μm. In much larger aperture fractures, much thicker water films can develop under slightly positive pressure potentials, resulting in free surface flow [*Kapoor*, 1994].

2. Lower Matric Potential Limit

The lower matric potential (Ψ_L) limit is associated with the condition where the rock matrix immediately underlying the fracture surface is just effectively saturated (satiated). As previously mentioned, hysteresis in the moisture characteristic relation prevents identification of a unique satiation energy, but as a starting point, the air-entry matric potential, Ψ_e, is taken as the threshold above which films might begin to develop on fracture surfaces (Figure 2). Note that if a system is rewetting from an unsaturated state, a higher matric potential (Ψ_S) is needed to reach the satiated state. In general, $\Psi_e < \Psi_L < \Psi_S$. It will be useful to correlate the air-entry matric potential to a more commonly measured property of the rock matrix. Two possible candidate properties are the porosity and the permeability. The possibility of using porosity as the correlating parameter was dismissed because the air-entry matric potential depends strongly on the characteristic pore-size not the porosity. Permeability is the preferred correlating parameter because, like the air-entry matric potential, it too depends very much on characteristic pore size [*Miller and Miller*, 1956; *Campbell*, 1985]. Differences in microscale structure (pore-scale geometry and pore size distribution), hysteresis in the rock matrix moisture characteristic relation, air entrapment within the matrix, and varying reliability of measurements all prevent identification of unique relations between permeabilities and air-entry matric potentials. However, we are only seeking to identify approximate values of air-entry matric potentials.

A survey of literature containing data on hydraulic properties for specific materials was conducted to compile information on porosities, air-entry matric potentials, and (saturated) permeabilities. Specific materials, their properties, and sources used are listed in Table 1. The various media listed include soils of various texture classes, rocks, ceramics, and glass bead packs. Only references that clearly identified air-entry matric potential values or that had sufficiently refined moisture characteristic relations such that interpolated values would be reliable were included in this list. Complications in defining the air-entry matric potential arise because the transition from tension-satiated conditions to partially desaturated states is very gradual for media with polydispersed, fine-scale pores, and because the identification of the air-entry matric potential is dependent on measurement resolution. Volume changes in finer-textures soils and heterogeneity within samples also contribute to deviations from ideal measurements on rigid, homogeneous porous media. For purposes of this survey, the air-entry energy was assigned to the main drainage curve matric potential associated with a 3% decrease in saturation relative to the satiated state. For references in which results were presented as tabulations of *van Genuchten* [1980] parameters, the air-entry matric potential of a given sample was estimated

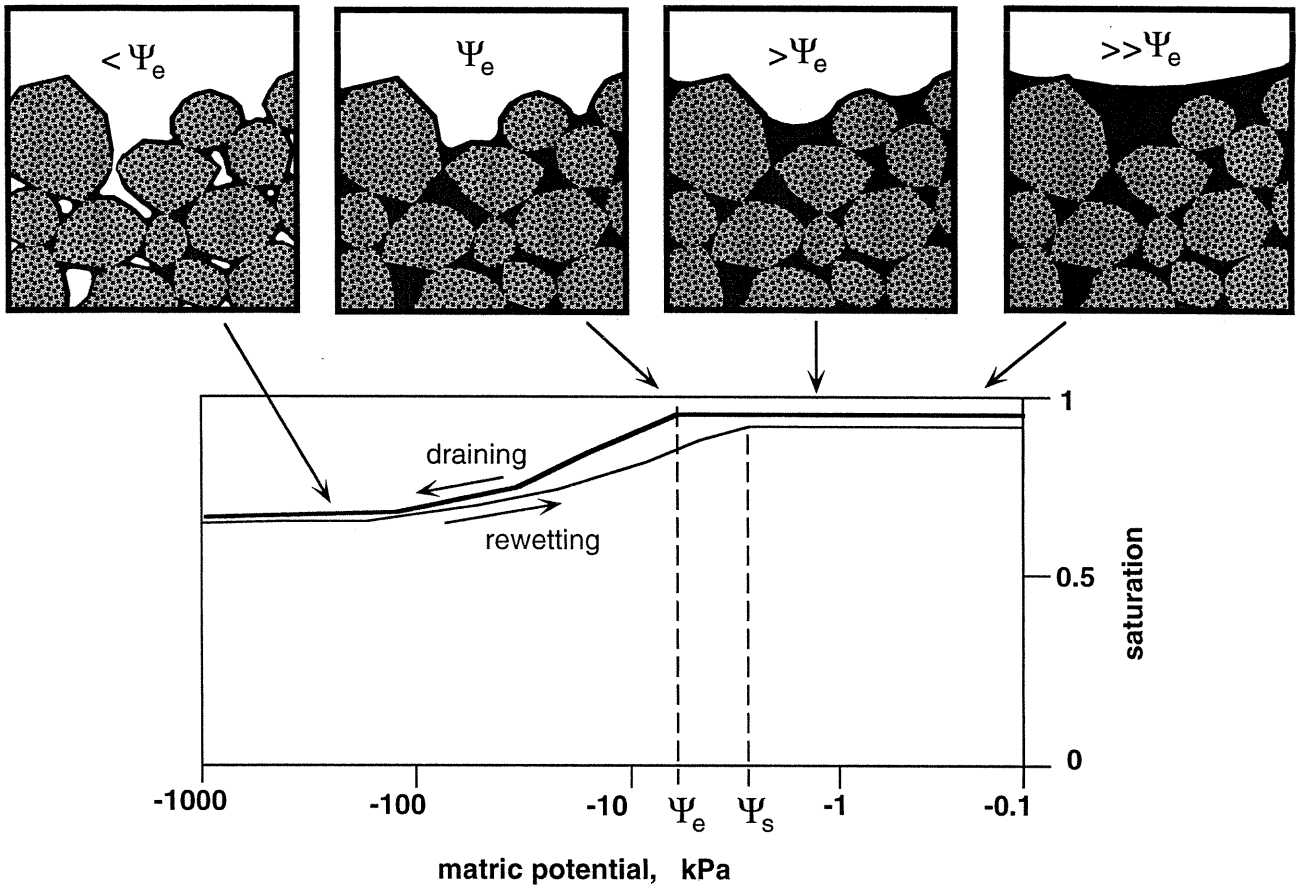

Figure 2. Conceptual model for development of thick water films on rough surfaces of fractured porous media. As the matric potential rises toward zero, the rock matrix becomes satiated at an energy between ψ_e and ψ_s, with hysteresis preventing identification of a unique value. At energies closer to zero, water films expand outward into the fracture surface by filling progressively larger depressions.

from an effective saturation of 97%, using the reported van Genuchten alpha and n values. The collected list includes 117 data pairs, spanning 9 orders of magnitude in permeability. A scatter plot of this data set shows a rough correlation (Figure 3). Included in this plot is a power law correlation curve of the form

$$\psi_e = -Ck^{-a}, \tag{1}$$

where k is the permeability and a and C are fitting parameters. The best-fit, power-law curve (heavy solid line in Figure 3) is obtained with $a = 0.32$ and $C = C_1 = 0.65$ Pa m$^{0.64}$. This correlation ($r^2 = 0.59$) predicts the air-entry matric potential to within 1 order of magnitude for 95% of the data set. The fine solid lines represent ±95% confidence interval slopes, and the fine dotted lines are order of magnitude bounds. Expected poorer correlations for power-law fits of air-entry matric potential versus porosity ($r^2 = 0.24$), and of porosity versus permeability ($r^2 = 0.36$) were obtained from the same data set (Table 1).

It is of interest to compare the power-law regression relation between air-entry matric potential and permeability to predictions based on scaling theories. The classic work on similitude by *Miller and Miller* [1956] is a systematic analysis of geometric scaling in unsaturated porous media and has served as the basis for a variety of more generalized methods applicable to spatially varying field settings [*Hillel and Elrick*, 1990]. Miller-Miller scaling starts with the approximation that porous media are geometrically similar, such that they differ primarily through differences in their characteristic length scales but retain a common porosity and pore geometry. The pore-scale hydrostatics and hydrodynamics are assumed controlled by surface tension and laminar flow. On this basis, the scaled matric (capillary) potential for a given system at a given saturation is directly proportional to its characteristic length (e.g., particle size or pore size), and the scaled hydraulic conductivity is inversely proportional to the characteristic length squared. Systems that differ primarily through differences in microscopic characteristic length scales are unified into single, universal scaled relations through this procedure. For Miller-Miller similar porous media, Ψ_e, is related to the permeability through (1), with $a = 0.5$ [*Miller and Miller*, 1956; *Campbell*, 1985]. The best-fit value of $a = 0.32$ for the power function fit (Figure 3) departs from Miller-Miller similitude, an anticipated result given the very wide diversity of materials included in the regression. Nevertheless, power-law relations with $a = 0.5$ can be fit through the data set, as shown in the dashed line in Figure 3. While pore geometry is expected to vary among these materials, the obvious departure from Miller-Miller similitude requirements comes through the very wide range of porosities (0.02–0.59) included in the data set.

Sposito and Jury [1990] developed a more general scaling analysis from the less restrictive condition of similarity in pore-

Table 1. Porosities, Permeabilities, and Air-Entry Matric Potentials of Various Porous Media

Source	Material	n	k, m^2	$-\Psi e$, $-Pa$
Moore [1939]	Oakley sand	0.43	1.0E − 13[a]	4.0E + 03
	Yolo fine sandy loam	0.52	4.0E − 14	4.0E + 03
	Yolo clay	0.52	9.0E − 15	4.0E + 03
	Yolo light clay	0.51	1.3E − 14	8.0E + 02
Luthin and Day [1955]	Oso Flaco fine sand	?	1.8E − 11	1.7E + 03
Klute and Wilkinson [1958]	104–125 μm sand	0.38	7.0E − 12	7.0E + 03
	149–177 μm sand	0.38	1.4E − 11	5.0E + 03
	210–250 μm sand	0.37	3.0E − 11	3.8E + 03
Hanks and Bowers [1962]	Sarpy loam	0.41	1.4E − 12	1.0E + 03
	Geary silt loam	0.46	1.0E − 13	2.0E + 03
Elrick and Bowman [1964]	Guelph loam	0.52	3.3E − 13	4.0E + 03
Jackson et al. [1965]	sand, 50–500 μm	0.40	5.1E − 12	4.6E + 03
	Adelanto loam	0.42	5.0E − 14	1.1E + 04
Watson [1966]	Botany sand	0.35	1.9E − 11	4.0E + 03
Topp and Miller [1966]	glass beads	0.33	1.0E − 11	4.3E + 03
Bybordi [1968]	fine sand, 150–250 μm	0.39	1.8E − 11	2.0E + 03
	coarse sand, 250–350 μm	0.38	4.0E − 11	1.3E + 03
Topp [1969]	Rubicon sandy loam	0.46	8.3E − 13	7.0E + 03
Poulovassilis [1970]	porous body 1, sand	0.27	1.7E − 11	1.5E + 03
Talsma [1970]	Adelaide dune sand	0.40	1.8E − 12	6.0E + 03
Topp [1971]	Rideau clay loam	0.42	2.5E − 12	3.0E + 03
	Caribou silt loam	0.44	2.5E − 13	9.0E + 03
Vachaud and Thony [1971]	sand	0.36	2.2E − 12	2.2E + 03
Arya et al. [1975]	Waukegan loam, 0.0–0.1 m	0.46	5.6E − 15	6.0E + 03
	Waukegan loam, 0.5–0.6 m	0.40	1.2E − 14	5.0E + 03
Gillham et al. [1976]	dune sand	0.31	5.8E − 12	2.5E + 03
Vauclin et al. [1979]	sand, 100–500 μm	0.33	9.7E − 12	1.9E + 03
van Genuchten [1980]	Hygiene sandstone	0.25	1.3E − 12	1.0E + 04
	Touchet silt loam	0.47	3.5E − 12	1.5E + 04
	Beit Netofa clay	0.45	9.8E − 16	1.0E + 04
Scotter and Clothier [1983]	repacked fine sand	0.45	2.0E − 12	2.0E + 03
Koorevaar et al. [1983]	medium fine sand	0.35	2.3E − 12	3.0E + 03
	loam	0.50	4.6E − 14	7.0E + 03
Peters et al. [1984]	Yucca Mtn. Tuff gu3-2	0.13	7.0E − 20	3.0E + 05
	Yucca Mtn. Tuff gu3-3	0.09	2.7E − 19	1.2E + 06
	Yucca Mtn. Tuff gu3-6	0.59	1.6E − 13	3.0E + 05
	Yucca Mtn. Tuff gu3-7	0.40	3.9E − 14	4.7E + 05
	Yucca Mtn. Tuff gu3-8	0.43	3.5E − 14	3.5E + 05
	Yucca Mtn. Tuff gu3-10	0.02	1.5E − 18	1.3E + 06
	Yucca Mtn. Tuff gu3-12	0.33	3.2E − 16	3.5E + 05
	Yucca Mtn. Tuff gu3-14	0.46	2.7E − 14	3.5E + 05
	Yucca Mtn. Tuff gu3-15	0.43	2.6E − 15	2.0E + 05
	Yucca Mtn. Tuff gu3-16	0.47	7.9E − 15	4.0E + 05
	Yucca Mtn. Tuff gu3-17	0.39	6.9E − 16	3.5E + 05
	Yucca Mtn. Tuff gu3-18	0.32	1.3E − 16	2.0E + 05
Puckett et al. [1985]	Lucedale Ap, sandy loam	0.40	1.8E − 13	3.2E + 03
	Troup E3, loamy sand	0.42	2.3E − 12	2.2E + 03
	Cahaba BC, sandy loam	0.37	3.5E − 13	3.2E + 03
	Malbis 1 Bt3, sandy clay loam	0.38	3.5E − 15	1.0E + 04
Stephens and Rehfeldt [1985]	fine fluvial sand	0.36	2.0E − 11	2.5E + 03
Anderson and Cassel [1986]	sandy loam	0.44	2.0E − 10	3.0E + 02
Flint and Flint [1990]	Yucca Mtn. Tuff 18A	0.28	2.0E − 19	1.5E + 05
	Yucca Mtn. Tuff 4-6	0.29	8.0E − 14	1.0E + 04
	Yucca Mtn. Tuff 17A	0.29	1.5E − 17	2.0E + 04
	Yucca Mtn. Tuff IV	0.44	1.8E − 14	1.0E + 04
Rasmussen et al. [1990]	Apache Leap Tuff x1-af	0.15	1.4E − 16	3.0E + 04
	Apache Leap Tuff x1-ag	0.14	1.5E − 16	3.0E + 04
	Apache Leap Tuff x2-cd	0.13	7.0E − 17	2.0E + 04
	Apache Leap Tuff x2-cn	0.16	2.7E − 16	3.5E + 04
	Apache Leap Tuff x3-eh	0.14	5.6E − 16	3.0E + 04
	Apache Leap Tuff x3-es	0.15	4.3E − 16	3.5E + 04
	Apache Leap Tuff y1-gb	0.14	1.7E − 16	1.5E + 04
	Apache Leap Tuff y1-gh	0.14	2.4E − 16	1.5E + 04
	Apache Leap Tuff y2-jf	0.13	2.0E − 16	2.5E + 04
	Apache Leap Tuff y2-jn	0.17	3.5E − 16	3.0E + 04
	Apache Leap Tuff y3-ms	0.17	3.9E − 16	3.5E + 04
	Apache Leap Tuff y3-mu	0.16	1.4E − 16	4.0E + 04
	Apache Leap Tuff z2-sk	0.13	3.5E − 16	4.5E + 04
	Apache Leap Tuff z2-sp	0.19	8.1E − 16	3.0E + 04
	Apache Leap Tuff z3-up		3.7E − 16	3.0E + 04
	Apache Leap Tuff z3-uu	0.14	4.3E − 16	3.0E + 04

Table 1. (continued)

Source	Material	n	k, m^2	$-\Psi e$, $-$Pa
Fayer and Gee [1992]	sand (91%)	0.42	8.0E − 12	1.0E + 03
Stephens [1992]	fluvial sand	0.34	2.0E − 11	1.5E + 03
	fluvial sand	0.27	6.0E − 12	2.0E + 03
	fluvial sand	0.35	3.0E − 12	1.7E + 03
Rawls et al. [1992]	sand	0.44	5.8E − 12	1.6E + 03
	loamy sand	0.44	1.7E − 12	2.1E + 03
	sandy loam	0.45	7.2E − 13	3.0E + 03
	loam	0.46	3.7E − 13	4.0E + 03
	silt loam	0.50	1.9E − 13	5.1E + 03
	sandy clay loam	0.40	1.2E − 13	5.9E + 03
	clay loam	0.46	6.4E − 14	5.6E + 03
	silty clay loam	0.47	4.2E − 14	7.0E + 03
	sandy clay loam	0.43	3.3E − 14	8.0E + 03
	silty clay loam	0.48	2.5E − 14	7.7E + 03
	clay loam	0.48	1.7E − 14	8.6E + 03
Shouse et al. [1992]	Etiwanda sand	0.39	1.3E − 12	1.6E + 03
Sisson and van Genuchten [1992]	Troup loamy sand	0.32	2.8E − 12	2.0E + 03
	Bethany loam	0.44	1.7E − 14	2.5E + 03
Rasmussen et al. [1993]	Apache Leap Tuff	0.17	1.7E − 15	1.0E + 05
Soilmoisture Equipment Corp. [1996]	0.5 bar high flow ceramic	0.50	3.1E − 14	5.5E + 04
	1 bar high flow ceramic	0.45	8.6E − 15	1.7E + 05
	1 bar ceramic	0.34	7.6E − 16	1.7E + 05
	2 bar ceramic	0.38	6.3E − 16	3.0E + 05
	2 bar high flow ceramic	0.38	6.9E − 16	3.0E + 05
	3 bar ceramic	0.34	2.5E − 16	4.0E + 05
	5 bar ceramic	0.31	1.2E − 16	5.6E + 05
	15 bar ceramic	0.32	2.6E − 18	1.6E + 06
Wan and Tokunaga [1997]	coarse sand	0.34	9.5E − 11	1.0E + 03
	medium sand	0.34	4.8E − 11	1.2E + 03
	fine sand	0.35	1.2E − 11	3.2E + 03
Shao and Horton [1998]	sandy loam	0.44	1.1E − 12	2.0E + 03
	silt loam	0.50	3.3E − 13	8.0E + 02
	loam	0.50	3.1E − 13	7.0E + 02
	sandy clay loam	0.54	5.3E − 14	2.0E + 03
	silty clay loam	0.56	1.1E − 14	2.0E + 03
	clay loam	0.57	2.2E − 14	2.0E + 03
Simunek et al. [1998]	silt loam	0.40	1.0E − 12	1.2E + 03
	loam	0.40	1.0E − 13	1.2E + 04
Flint [1998]	Yucca Mtn. Tuff CW	0.08	5.0E − 18	2.0E + 05
	Yucca Mtn. Tuff BT3	0.41	5.0E − 15	1.0E + 04
	Yucca Mtn. Tuff TR	0.16	2.0E − 16	1.0E + 04
	Yucca Mtn. Tuff TUL	0.15	2.0E − 17	4.0E + 04
	Yucca Mtn. Tuff TMN	0.11	4.0E − 18	3.0E + 05
	Yucca Mtn. Tuff PV3	0.04	5.0E − 18	3.0E + 06
	Yucca Mtn. Tuff CHZ	0.33	5.0E − 18	7.0E + 04
	Yucca Mtn. Tuff PP2	0.26	3.0E − 17	3.0E + 04

[a]Read 1.0E − 13 as 1.0×10^{-13}.

size distribution. Thus their generalized scaling theory accommodates variability in porosity commonly found in soils and rock. The parameter a in (1) is equivalent to $1/\eta$ in the generalized scaling analysis of *Sposito and Jury* [1990]. The manner in which η relates to scale-invariance of the Richards equation is discussed by *Sposito and Jury* [1990] and by *Sposito* [1998]. It is interesting to note that $\eta = 3.1$ (from $a = 0.32$ in Figure 3) is in the same range as mean values obtained from analysis of two field soils used in the studies of *Jury et al.* [1987] and *Sposito and Jury* [1990]. Mean η values from their Hamra and Panoche soils are 3.36 and 2.54, respectively. The more restrictive condition for applicability of Miller-Miller similitude (i.e., geometric similitude) leads to $\eta = 2$.

Since the value of C_1 is based on data obtained from desaturation curves, it applies best to desaturation processes. During a resaturation process, the matric potential at which the rock becomes satiated is expected to be higher (closer to zero) than Ψ_e because of factors responsible for hysteresis in moisture characteristics [*Hillel*, 1980]. Since one does not generally know the wetting history of the medium of interest, a small improvement in the estimated lower matric potential threshold is obtained by choosing a smaller value of C. The magnitude of the wetting satiation matric potential (Ψ_s in Figure 2) is often about half that of Ψ_e [e.g., *Haines*, 1930; *Bouwer*, 1966; *Haverkamp and Parlange*, 1986]. Therefore setting C to 75% of C_1 will provide an estimate for Ψ_L that is about half way between Ψ_e and Ψ_s. Thus a value of $C_2 = 0.5$ Pa m$^{0.62}$ was selected and used in (1) to estimate Ψ_L.

As the matric potential is increased above the level predicted in (1) (using C_2), the air-water interface expands outward on rough surfaces by first filling finer-scale depressions and progressively filling larger-scale minima as zero matric potential is approached. In this progression, radii of curvature of free air-water interfaces (those surfaces not directly retracted against solid surfaces) are envisioned to increase in accordance with the Laplace-Young equation [*Philip*, 1978].

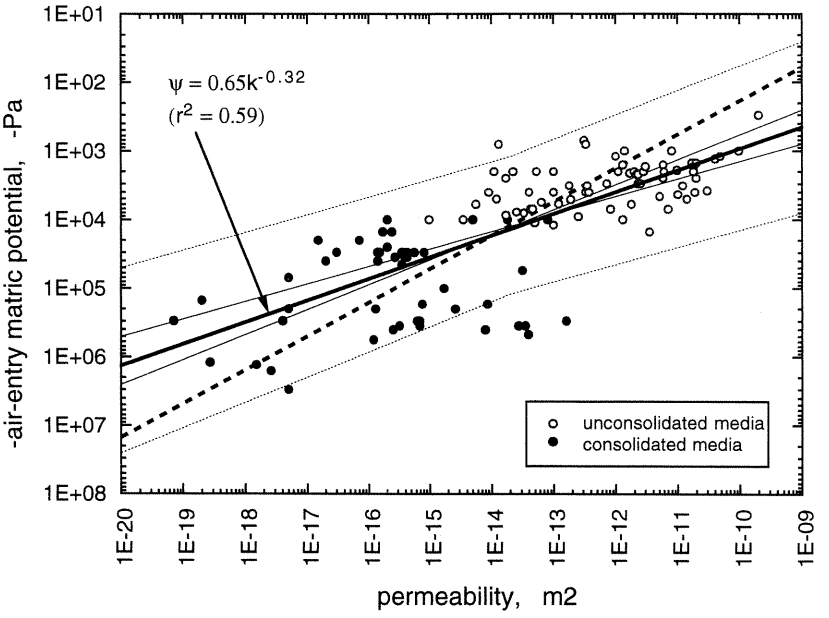

Figure 3. Correlation between permeability of porous media and air-entry matric potentials, based on data from Table 1. Open and filled points denote data from unconsolidated (soils, glass beads) and consolidated (rocks, ceramics) media, respectively. The heavy solid line is the power law function fit to all data ($a = 0.32$). The fine solid lines show ±95% confidence intervals for the power law slope, and the dotted lines indicate ±1 order of magnitude relative to the power law 95% confidence interval. An example of a power law relation with $a = 0.5$ is also shown as a heavy dashed line.

Since the magnitude of fracture surface roughness is typically greater than the characteristic pore size of the rock matrix, water films along fracture surfaces at matric potentials greater (closer to zero) than ψ_L are thick relative to films that occur at lower ψ within the bulk rock. Our analysis further assumes that the local surface roughness is small relative to the local aperture (as depicted in Figures 1 and 2). Where this condition is not met (especially around contact points between opposing fracture surfaces), local aperture saturation coincides with local film thickening.

3. Upper Matric Potential Limit

The upper limit in matric potential, Ψ_U, above which films are eliminated by water filling of the local aperture, will be approximated by the parallel plate capillary relation

$$\psi_u = -\frac{2\sigma}{b}, \tag{2}$$

where σ is the (air-water) surface tension and b is the fracture aperture (Figure 1). This condition for local fracture saturation is central to aperture-based conceptual models [*Wang and Narasimhan*, 1985]. The contact angle term is not included in (2) because we limit our analysis to only completely water-wetted fracture surfaces. The inverse dependence of Ψ_U on b is approximate because local variations in b, hysteresis in the matric potential dependence of fracture saturation [*Glass and Norton*, 1992; *Glass et al.*, 1996], in-plane air-water interfacial curvature [*Glass et al.*, 1998], and gas phase entrapment in fractures [*Nicholl et al.*, 2000] are all ignored. It should be noted that the upper matric potential limit becomes ambiguous for very large b because of the increasing influence of gravity on the shape of the air-water interface. An upper limit in b for applicability of (2) can be estimated from the ratio of gravitational to capillary forces acting on an air-water interface that bridges (fills) a fracture. This ratio is given by the Bond number,

$$Bo = \frac{\rho g b^2}{2\sigma}, \tag{3}$$

where ρ is the density of water and g is the acceleration due to gravity. Since Bo is quadratically dependent on b, and since $Bo = 0.27$ for $b = 2$ mm aperture, applicability of (2) degrades rapidly for larger aperture fractures. Although very large aperture fractures may not be amenable to capillary-based analysis of saturation criteria, they are capable of supporting fast film flow, given the necessary local potentials and gradients. Furthermore, such very large aperture fractures can accommodate free surface film flows.

4. Flow Regimes for Fractured Rock and the Domain of Stable Thick Films

Given the approximate validity of (1) and (2), we return to key questions concerning the conditions compatible with thick films on fracture surfaces. How much "room" in k-b-ψ parameter space does the domain of stable thick films occupy? Even if this domain is small, is it significant? A convenient way to examine the combined influences of matrix permeability, fracture aperture, and matric potential is illustrated in Figure 4. The base of this three-dimensional parameter space is defined by rock matrix permeability and fracture aperture axes, such that the local material properties of a given segment of fracture surface are defined by a point on this k-b plane. The vertical axis represents matric potential, with increasing (nearer to zero) values in the upward direction. Thus the hydraulic state at a given location on a fracture surface can be represented as

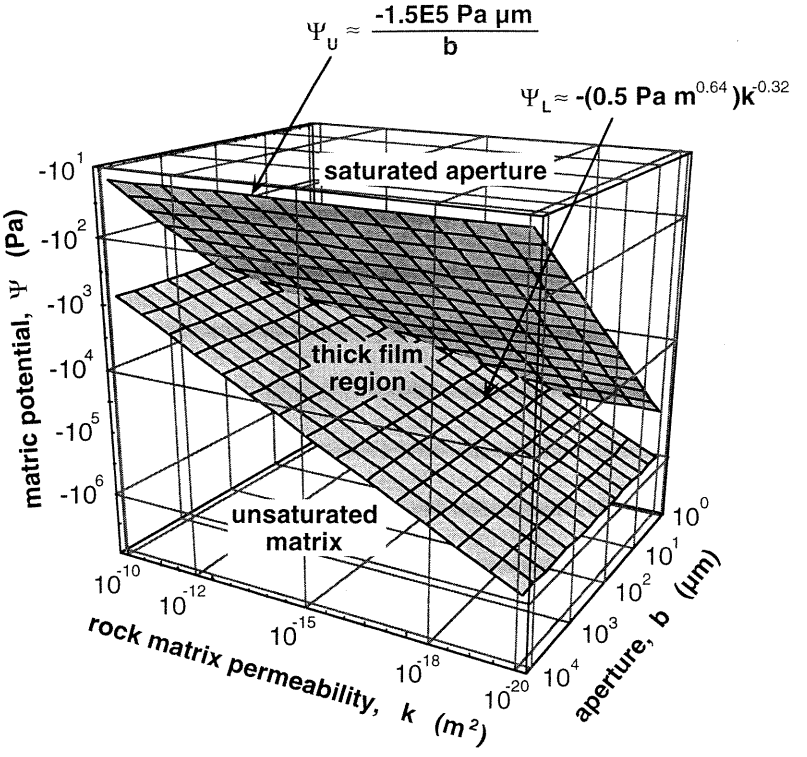

Figure 4. Approximate parameter space for the partitioning of water in fractured porous media, showing how rock matrix permeability, fracture aperture, and matric potential combine to determine whether a region is characterized by unsaturated matrix rock, by satiated matrix plus thick water films along fractures, or by full matrix and fracture saturation.

a point along a vertical line of constant k and b, with the point moving upward during wetting and downward during drying. Figure 4 illustrates how regions of stability for (1) unsaturated rock matrix, (2) satiated matrix coexisting with water films along fractures, and (3) saturated fractures can be approximately delineated based on information on matrix permeability, fracture aperture, and matric potential. The lower diagonal surface approximates the permeability-dependent satiation matric potential (equation (1), with $C_2 = 0.5$ Pa $m^{0.64}$ and $a = 0.32$), and the lower limit at which thick films develop along fracture surfaces. The location of the upper diagonal surface delimits the aperture-dependent transition from films to saturated fractures (equation (2)).

From the above analysis, thick films in rock fractures are restricted to k-b-ψ combinations occurring between the two diagonal surfaces shown in Figure 4. It is interesting to note that the thick film region comprises a significant portion of this parameter space for vadose zone rock (keeping in mind the logarithmic axes). In general, rock matrix permeabilities less than $\sim 10^{-14}$ m^2 and apertures greater than about 30 μm permit some matric potential range over which thick water films are stable. This does not imply that fast film flow can occur over this entire thick film region, an issue we consider later. Examination of Figure 4 also shows that for regions of large aperture (approximately for $b > 100$ μm), thick films can develop on rock surfaces over wide ranges of matrix permeabilities (approximately $k < 10^{-12}$ m^2), given sufficient high matric potentials. In the limit of very large aperture values, this result is relevant to the problems of vadose zone flow into caves, and also to flows associated with seepage faces in surface hydrology. Although (2) does not apply in such environments, these types of processes clearly express the local importance of film flow.

The analysis resulting in Figure 4 also shows that certain combinations of k and b (the region "behind" the intersection of the two bounding surfaces) preclude development of thick films along fracture surfaces. This prohibited region is associated with fracture apertures that are too narrow to permit film flow because the matric potential needed to effectively saturate the matrix is already also sufficient to saturate the fracture. A very narrow aperture fracture in coarse, high permeability sandstone is an example of a system where thick films along an unsaturated fracture could not develop.

Although we have delineated the approximate range over which thick water films exist in k-b-ψ space, a related practical issue remains to be resolved. This yet unresolved problem is the determination of what subregion of the thick film stability region is associated with "fast" film flow. The answer to this question depends on the definition of fast flow, the inclination of the fracture surface, and the nature of the fracture surface roughness (which controls film hydraulic properties). The definition of fast film flow is context-dependent, and we have used >10 m yr^{-1} as an order-of-magnitude demarcation that can be relevant in vadose zone contaminant transport. The dependence of film thicknesses and velocities on fracture surface roughness and matric potential is anticipated to be complex. Direct measurements of film flow on well-defined surfaces are still needed, and we are conducting experiments to obtain such measurements as part of a related study. The results to date [*Tokunaga and Wan*, 1997; *Tokunaga et al.*, 2000] indicated that only the upper portion of the thick film stability field, associated with matric potentials greater (less negative) than about

-1 kPa, will permit fast (>10 m yr^{-1}) film flow in fractures. Thus a horizontal boundary at around $\psi = -1$ kPa in the thick film domain of Figure 4 might be added to delineate high versus low transmissivity films. Calculations of film transmissivities for a reasonable range of fracture surface topographies will improve our ability to predict conditions necessary for fast film flow [*Or and Tuller*, 2000]. The smaller subdomain of highly transmissive films is important because of the fact that high unsaturated fracture flow rates occur in this region.

5. Summary

Flow through unsaturated fractured rock occurs via a number of processes, including film flow. Approximate ranges of conditions necessary for the presence of thick water films along unsaturated fracture surfaces were investigated through considering rock matrix and fracture aperture saturation criteria. Thick films exists when the matric potential is high enough to effectively saturate (satiate) the immediately underlying rock matrix, yet low enough not to saturate the local fracture aperture. The lower energy limit for stable thick films was estimated through correlations between air-entry matric potentials and matrix permeabilities. The upper matric potential limit was estimated from the Laplace-Young predicted inverse fracture aperture dependence of capillary filling. With these two limiting relations, the domain for stable thick films was identified in the parameter space defined by matrix permeability, fracture aperture, and matric potential. These results show that thick films occur over a moderate range of matric potentials when the rock matrix permeability is less than $\sim 10^{-14}$ m^2 and the fracture aperture is greater than ~ 30 μm. Such combinations of permeabilities and apertures are common in fractured rock vadose zones. Thus thick water films can form in these environments within the matric potential ranges identified here. It is important to keep in mind that near-zero matric potentials are necessary for the possible development of fast film flow.

Acknowledgments. Helpful internal review comments by Garrison Sposito (University of California, Berkeley, and LBNL) and final review comments by Robert Glass (Sandia National Laboratories), Associate Editor Scott Tyler (University of Nevada, Reno), and an anonymous reviewer are gratefully acknowledged. This work was carried out under U.S. Department of Energy Contracts DE-AC03-76SF00098, with funding provided by the U.S. Department of Energy, Basic Energy Sciences, Geosciences Research Program.

References

Anderson, S. H., and D. K. Cassel, Statistical and autoregressive analysis of soil physical properties of Portsmouth sandy loam, *Soil Sci. Soc. Am. J.*, *50*, 1096–1104, 1986.

Arya, L. M., D. A. Farrell, and G. R. Blake, A field study of soil water depletion patterns in presence of growing soy bean roots, 1, Determination of hydraulic properties of the soil, *Soil Sci. Soc. Am. Proc.*, *39*, 424–430, 1975.

Bouwer, H., Rapid field measurement of air-entry value and hydraulic conductivity of soil as significant parameters in flow system analysis, *Water Resour. Res.*, *2*, 729–738, 1966.

Bybordi, M., Moisture profiles in layered porous materials during steady-state infiltration, *Soil Sci.*, *105*, 379–383, 1968.

Campbell, G. S., *Soil Physics with BASIC*, *Dev. Soil Sci.*, vol. 14, 150 pp., Elsevier Sci., New York, 1985.

Elrick, D. E., and D. H. Bowman, Note on an improved apparatus for soil moisture flow measurements, *Soil Sci. Soc. Am. Proc.*, *27*, 450–453, 1964.

Fayer, M. J., and G. W. Gee, Predicting drainage at a semiarid site: Sensitivity to hydraulic property description and vapor flow, in *Indirect Methods for Estimating the Hydraulic Properties, of Unsaturated Soils*, edited by M. T. van Genuchten, F. J. Leij, and L. J. Lund, pp. 609–619, U.S. Salinity Lab., U.S. Dep. of Agric., Riverside, Calif., 1992.

Flint, L. E., Characterization of hydrogeologic units using matrix properties, Yucca Mountain, Nevada, *U.S. Geol. Surv. Water Resour. Invest. Rep. 97-4243*, 1998.

Flint, L. E., and A. L. Flint, Preliminary permeability and water-retention data from nonwelded and bedded tuff samples, Yucca Mountain, Nye County, Nevada, *U.S. Geol. Surv. Open File Rep. 90-569*, 1990.

Gillham, R. W., A. Klute, D. F. Heermann, Hydraulic properties of a porous medium: Measurement and empirical representation, *Soil Sci. Soc. Am. J.*, *40*, 203–207, 1976.

Glass, R. J., and D. L. Norton, Wetted-region structure in horizontal unsaturated fractures: Water entry through the surrounding porous matrix, paper presented at 3rd International Conference High Level Radioactive Waste Management, Am. Nucl. Soc., Las Vegas, Nev., April 12–16, 1992.

Glass, R. J., M. J. Nicholl, and V. C. Tidwell, Challenging and improving conceptual models for isothermal flow in unsaturated, fractured rock through exploration of small-scale processes, *Rep. SAND95-1824, UC-814*, Sandia Natl. Lab., Albuquerque, N. M., 1996.

Glass, R. J., M. J. Nicholl, and L. Yarrington, A modified invasion percolation model for low-capillary number immiscible displacements in horizontal rough-walled fractures: Influence of local in-plane curvature, *Water Resour. Res.*, *34*, 3215–3234, 1998.

Haines, W. B., Studies in the physical properties of soil, V, The hysteresis effect in capillary properties, and the modes of moisture distribution associated therewith, *J. Agric. Sci.*, *20*, 97–116, 1930.

Hanks, R. J., and S. A. Bowers, Numerical solution of the moisture flow equation for infiltration into layered soils, *Soil Sci. Soc. Am. Proc.*, *26*, 530–534, 1962.

Haverkamp, R., and J.-Y. Parlange, Predicting the water-retention curve from particle-size distribution, 1, Sandy soils without organic matter, *Soil Sci.*, *142*, 325–339, 1986.

Hillel, D., *Fundamentals of Soil Physics*, Academic, San Diego, Calif., 1980.

Hillel, D., and D. E. Elrick, *Scaling in Soil Physics: Principles and Applications*, *Spec. Publ. 25*, Soil Sci. Soc. Am., Madison, Wisc., 1990.

Jackson, R. D., R. J. Reginato, and C. H. M. van Bavel, Comparison of measured and calculated hydraulic conductivities of unsaturated soils, *Water Resour. Res.*, *1*, 375–380, 1965.

Jury, W. A., D. Russo, and G. Sposito, The spatial variability of water and solute transport properties in unsaturated soil, II, Scaling models of water transport, *Hilgardia*, *55*, 33–56, 1987.

Kapoor, V., Water film flow in a fracture in unsaturated porous medium, *Rep. CNWRA 94-009*, Cent. for Nucl. Waste Regulatory Anal., San Antonio, Tex., 1994.

Klute, A., Water Retention: Laboratory Methods, in *Methods of Soil Analysis*, part 1, *Physical and Mineralogical Methods*, *Agron. Monogr.*, vol. 9, 2nd ed., pp. 635–662, Am. Soc. Agron., Madison, Wisc., 1986.

Klute, A., and G. E. Wilkinson, Some tests of the similar media concept of capillary flow, 1, Reduced capillary conductivity and moisture characteristic data, *Soil Sci. Soc. Am. Proc.*, *22*, 278–281, 1958.

Koorevaar, P., G. Menelik, and C. Dirksen, *Elements of Soil Physics*, *Dev. Soil Sci.*, vol. 13, 228 pp., Elsevier Sci., New York, 1983.

Luthin, J. N., and P. R. Day, Lateral flow above a sloping water table, *Soil Sci. Soc. Am. Proc. 18*, 406–410, 1955.

Miller, E. E., and R. D. Miller, Physical theory for capillary flow phenomena, *J. Appl. Phys.*, *4*, 324–332, 1956.

Moore, R. E., Water conduction from shallow water tables, *Hilgardia*, *12*, 383–425, 1939.

Muller, H. J., Extraordinarily thick water films on hydrophilic solids: A result of hydrophobic repulsion?, *Langmuir*, *14*, 6789–6792, 1998.

Nicholl, M. J., R. J. Glass, and S. W. Wheatcraft, Gravity-driven infiltration instability in initially dry nonhorizontal fractures, *Water Resour. Res.*, *30*, 2533–2546, 1994.

Nicholl, M. J., H. Rajaram, and R. J. Glass, Factors controlling satiated relative permeability in a partially-saturated horizontal fracture, *Geophys. Res. Lett.*, *27*, 393–396, 2000.

Nitao, J., and T. Buscheck, Infiltration of a liquid front in an unsatur-

ated fractured porous medium, *Water. Resour. Res.*, *27*, 2099–2112, 1991.

Or, D., and M. Tuller, Flow in unsaturated porous media: Hydraulic conductivity of rough surfaces, *Water Resour. Res.*, *36*, 1165–1177, 2000.

Pashley, R. M., Multilayer adsorption of water on silica: An analysis of experimental results, *J. Colloid Interface Sci.*, *78*, 246–248, 1980.

Peters, R. R., E. A. Klavetter, I. J. Hall, S. C. Blair, P. R. Heller, and G. W. Gee, Fracture and matrix hydrologic characteristics of tuffaceous materials from Yucca Mountain, Nye County, Nevada, *Rep. SAND84-1471*, Sandia Natl. Lab., Albuquerque, N. M., 1984.

Philip, J. R., Adsorption and capillary condensation on rough surfaces, *J. Phys. Chem.*, *82*, 1379–1385, 1978.

Poulovassilis, A., Hysteresis of pore water in granular porous bodies, *Soil Sci.*, *109*, 5–12, 1970.

Puckett, W. E., J. H. Dane, and B. F. Hajek, Physical and mineralogical data to determine soil hydraulic properties, *Soil Sci. Soc. Am. J.*, *49*, 831–836, 1985.

Rasmussen, T. C., D. D. Evans, P. J. Sheets, and J. H. Banford, Unsaturated Fractured Rock Characterization Methods and Data Sets at the Apache Leap Tuff Site, *Rep. NUREG/CR-5596*, Dep. Hydrol. and Water Resour., Univ. of Ariz., Tucson, 1990.

Rasmussen, T. C., D. D. Evans, P. J. Sheets, and J. H. Blanford, Permeability of Apache Leap Tuff: Borehole and core measurements using air and water, *Water Resour. Res.*, *29*, 1997–2006, 1993.

Rawls, W. J., L. R. Ahuja, and D. L. Brakensiek, Estimating soil hydraulic properties from soils data, in *Indirect Methods for Estimating the Hydraulic Properties of Unsaturated Soils*, edited by M. T. van Genuchten, F. J. Leij, and L. J. Lund, pp. 329–340, U.S. Salinity Lab., U.S. Dep. of Agric., Riverside, Calif., 1992.

Scotter, D. R., and B. E. Clothier, A transient method for measuring soil water diffusivity and unsaturated hydraulic conductivity, *Soil Sci. Soc. Am. J.*, *47*, 1068–1072, 1983.

Shao, M., and R. Horton, Integral method for estimating soil hydraulic properties, *Soil Sci. Soc. Am. J.*, *62*, 585–592, 1998.

Shouse, P. J., J. B. Sisson, G. de Rooij, J. A. Jobes, and M. T. Van Genuchten, Application of fixed-gradient methods for estimating soil hydraulic conductivity, in *Indirect Methods for Estimating the Hydraulic Properties of Unsaturated Soils*, edited by M. T. van Genuchten, F. J. Leij, and L. J. Lund, pp. 675–684, U.S. Salinity Lab., U.S. Dep. of Agric., Riverside, Calif., 1992.

Simunek, J., O. Wendroth, M. T. van Genuchten, Parameter estimation analysis of the evaporation method for determination of soil hydraulic properties, *Soil Sci. Soc. Am. J.*, *62*, 894–905, 1998.

Sisson, J. B., and M. T. van Genuchten, Estimation of hydraulic conductivity without computing fluxes, in *Indirect Methods for Estimating the Hydraulic Properties of Unsaturated Soils*, edited by M. T. van Genuchten, F. J. Leij, and L. J. Lund, pp. 665–674, U.S. Salinity Laboratory, U.S. Dep. of Agric., Riverside, Calif., 1992.

Soilmoisture Equipment Corp., Porous ceramics, 600 series, Santa Barbara, Calif., 1996.

Sposito, G., Scale invariance and the Richards equation, in *Scale Dependence and Scale Invariance in Hydrology*, edited by G. Sposito, pp. 167–189, Cambridge Univ. Press, New York, 1998.

Sposito, G., and W. A. Jury, Miller similitude and generalized scaling analysis, in *Scaling in Soil Physics, Principles and Applications*, *Spec. Publ. 25*, Soil Sci. Soc. of Am., Madison, Wisc., 1990.

Stephens, D. B., A comparison of calculated and measured unsaturated hydraulic conductivity of two uniform soils in New Mexico, in *Indirect Methods for Estimating the Hydraulic Properties of Unsaturated Soils*, edited by M. T. van Genuchten, F. J. Leij, and L. J. Lund, pp. 249–261, U.S. Salinity Lab., U.S. Dep. of Agric., Riverside, Calif., 1992.

Stephens, D. B., and K. R. Rehfeldt, Evaluation of closed-form analytical models to calculate conductivity in a fine sand, *Soil Sci. Soc. Am. J.*, *49*, 12–19, 1985.

Su, G. W., J. T. Geller, K. Pruess, and F. Wen, Experimental studies of water seepage and intermittent flow in unsaturated, rough-walled fractures, *Water Resour. Res.*, *35*, 1019–1037, 1999.

Talsma, T., Hysteresis in two sands and the independent domain model, *Water Resour. Res.*, *6*, 964–970, 1970.

Tokunaga, T. K., and J. Wan, Water film flow along fracture surfaces of porous rock, *Water Resour. Res.*, *33*, 1287–1295, 1997.

Tokunaga, T. K., J. Wan, and S. R. Sutton, Transient film flow on rough fracture surfaces, *Water Resour. Res.*, *36*, 1737–1746, 2000.

Topp, G. C., Soil-water hysteresis measured in a sandy loam and compared with the hysteretic domain model, *Soil Sci. Soc. Am. Proc.*, *33*, 645–651, 1969.

Topp, G. C., Soil water hysteresis in silt loam and clay loam soils, *Water Resour. Res.*, *7*, 914–920, 1971.

Topp, G. C., and E. E. Miller, Hysteretic moisture characteristics and hydraulic conductivities for glass beads, *Soil Sci. Soc. Am. Proc.*, *30*, 156–162, 1966.

Vachaud, G., and J. L. Thony, Hysteresis during infiltration and redistribution in a soil column, *Water Resour. Res.*, *7*, 111–127, 1971.

van Genuchten, M. T., A closed form equation for predicting the hydraulic conductivity of unsaturated soils, *Soil Sci. Soc. Am. J.*, *44*, 892–898, 1980.

Vauclin, M., D. Khanji, and G. Vachaud, Experimental and numerical study of a transient, two-dimensional, unsaturated-saturated water table recharge problem, *Water Resour. Res.*, *15*, 1089–1101, 1979.

Wang, J. S. Y., and T. N. Narasimhan, Hydrologic mechanisms governing fluid flow in a partially saturated, fractured, porous medium, *Water Resour. Res.*, *21*, 1861–1874, 1985.

Wang, J. S. Y., N. G. W. Cook, H. A. Wollenberg, C. L. Carnahan, I. Javandel, and C. F. Tsang, Geohydrological data and models of Rainier Mesa and their implications to Yucca Mountain, in *High Level Radioactive Waste Management, Proceedings 4th Annual International Conference*, vol. 1, pp. 675–681, Am. Nucl. Soc., Las Vegas, Nev., 1993.

Watson, K. K., An instantaneous profile method for determining the hydraulic conductivity of unsaturated porous materials, *Water Resour. Res.*, *2*, 709–715, 1966.

T. K. Tokunaga and J. Wan, Earth Sciences Division, E. O. Lawrence Berkeley National Laboratory, 1 Cyclotron Road, MS 90-1116, Berkeley, CA 94720. (tktokunaga@lbl.gov)

(Received July 25, 2000; revised January 12, 2001;
accepted March 21, 2001.)